A Miniaturized Dual-Band MIMO Antenna for WLAN Applications

Muhammad Saeed Khan, Muhammad Farhan Shafique, *Member, IEEE*, Aftab Naqvi, Antonio-D Capobianco, *Member, IEEE*, Bilal Ijaz, and Benjamin D. Braaten, *Senior Member, IEEE*

***Abstract*—This letter reports on a compact planar dual-band Multiple-Input and Multiple-Output (MIMO) antenna for Wireless Local Area Network (WLAN) applications. The proposed antenna primarily consists of two meandered monopole radiators that are decoupled by introducing a folded Y-shape isolator element and it is shown that the edge coupling between the radiators and isolator introduces the resonance at the lower band. The miniaturization is achieved by passing the signal on to the bottom layer where a meandered line conductor introduces a broadside coupling with the radiator, originating the higher band resonance. The antenna operates between 2.4 GHz to 2.5 GHz and 5.45 GHz to 5.65 GHz with an isolation of more than 25 dB and 15 dB, respectively. The antenna measures only 19×23 mm^2.**

***Index Terms*—Diversity, envelope correlation co-efficient (ECC), multiple-input multiple-output (MIMO), wireless local area network (WLAN).**

I. Introduction

HIGH DATA RATES with a large signal-to-noise ratio in Wireless Local Area Networks (WLAN)s can be achieved by using multiple-input multiple-output (MIMO) antenna systems [1]. MIMO systems enhance data reliability by using multiple radiators at the transmitting and receiving ends. In order to ensure a minimum correlation in a rich scattering environment, the antenna elements must be kept isolated from the radiation of neighboring elements. On the other hand, it is very challenging to achieve high isolation and keep small antenna dimensions because of strong electromagnetic mutual coupling.

Manuscript received September 29, 2014; revised October 31, 2014; accepted December 19, 2014. Date of publication January 05, 2015; date of current version April 21, 2015.

M. S. Khan is with the Department of Electrical and Computer Engineering, North Dakota State University, Fargo, ND 58102 USA and also with the Department of Information Engineering of Padova University, Padova, 35100, Italy (e-mail: mskj786@hotmail.com).

M. F. Shafique and B. Ijaz are with the Center for Advanced Studies in Telecommunications, and also with the Department of Electrical Engineering, COMSATS IIT, Islamabad, 45000, Pakistan.

A.-D. Capobianco is with the Department of Information Engineering of Padova University, Padova, 35131, Italy.

A. Naqvi was with the Department of Electrical and Computer Engineering, North Dakota State University, Fargo ND 58102 USA. He is now with the Department of Electrical Engineering, COMSATS IIT, Sahiwal, 57000 Pakistan .

B. D. Braaten is with the Department of Electrical and Computer Engineering, North Dakota State University, Fargo, ND 58102 USA (e-mail:benbraaten@ieee.org) .

Color versions of one or more of the figures in this letter are available online at http://ieeexplore.ieee.org.

Digital Object Identifier 10.1109/LAWP.2014.2387701

Significant research work has been conducted to enhance the port-to-port isolation in order to improve the diversity performance of antenna systems [2]–[10]. Generally the isolation is achieved by modifying the ground plane by inserting slits and slots, hence modifying the current path [2][3]. Alternatively, Electromagnetic Band Gap (EBG) cells can be introduced to suppress coupling [4]. Defective ground structures [5][6], various neutralization methods [7][8], orthogonal feeding modes [9] and orthogonal elements [10] have also been investigated to achieve the optimum performance of a MIMO system.

The applications of MIMO systems are not limited to narrow band communications, a number of dual-band and ultra wide-band diversity antenna systems have been proposed. The dual band or wide-band operation does not allow the conventional resonant elements to be incorporated to suppress the surface waves and space waves, therefore alternative techniques such as multiple resonant decoupling structures or modified radiating elements have been used [11]–[13]. More specifically, in [12] a decoupling structure has been proposed on the back side of radiators which captures the coupling fields and converts them in to surface currents to reduce the mutual coupling between the antenna elements. But, the decoupling structure was not electrically connected to the antenna. Miniaturized antenna systems are the key to device compactness. More specifically for portable devices and for WLAN dongle applications, antenna footprints are very crucial due to limited room. In recent years a number of antenna designs have been proposed for wireless dongle applications [14]–[16]. However, the proposed antennas have either non-planar construction or they are large in size.

In this work, the highly miniaturized dual band diversity antenna in Fig. 1 is proposed, which is suitable for integration in handheld devices as well as in USB dongles. The proposed design consists of two printed meander-line antenna elements which are placed close to each other. Dual band operation of the proposed system is achieved by exploiting the edge and broadside coupling generated in the system as a result of introducing the folded Y-shape isolator and the meander line conductor on the bottom side of the substrate.

II. Two Element MIMO Antenna Design

The antenna in Fig. 1 consists of two meandered monopole radiators. A folded Y-shape isolator attached to the ground plane is placed between the radiators on the top side (as shown in the Fig. 1(a)) and the bottom side of the substrate consists of two meandered lines strips connected to the respective radiators through via holes to introduce broadside coupling with the radiators (as shown in Fig. 1(b)). The resonance at the higher band is achieved by passing the current to the meander line on

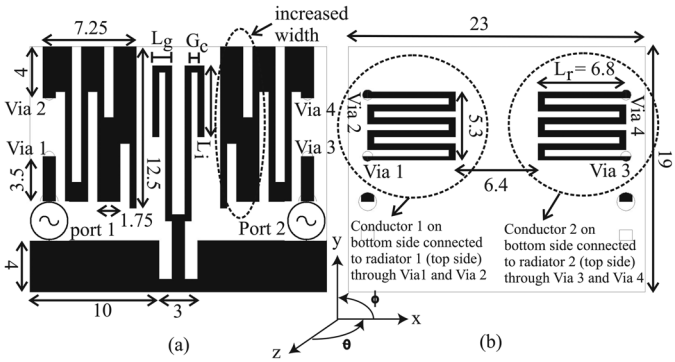

Fig. 1. Layout of final proposed design: (a) top view (b) bottom view ($L_g = 1.5$ mm, $G_c = 0.5$ mm, $L_i = 5.5$ mm and $L_r = 6.8$ mm).

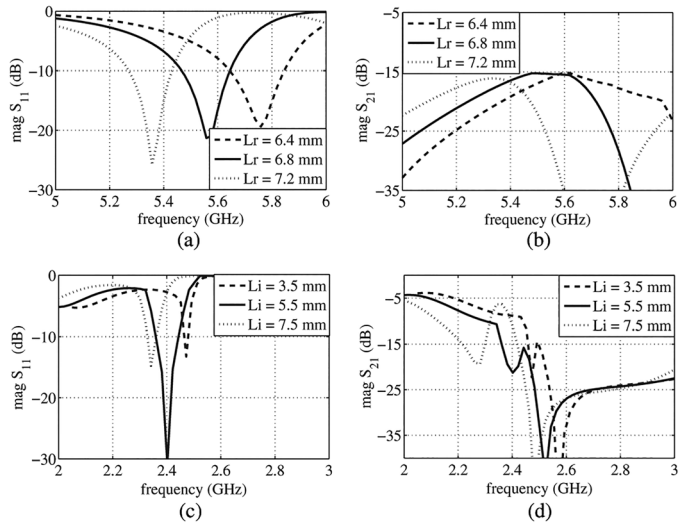

Fig. 2. Effect of the meander line conductor in the higher frequency band on (a) $|S_{11}|$ and (b) mutual coupling; and effect of the Y-shape folded stub in the lower frequency on (c) $|S_{11}|$ and (d) mutual coupling.

the bottom side through a via. A strong broadside coupling is generated between the meander line and the monopole radiator. The radiators are slightly modified at their edges towards the middle of the substrate by increasing the strip width (as encircled in the Fig. 1(a)) and the length of each meander line on the bottom layer is chosen to be between 0.5λ and 1.0λ, where λ is the wavelength of the 5.5 GHz operating band. This modification supports stronger broadside coupling with the meander line on the bottom side and optimum inductance between the lines of the radiator to achieve impedance matching.

For the lower band, the edge coupling between the monopole radiator and folded Y-shape isolator is utilized. The coupling can be controlled by varying the separation distance between the radiator and isolator. Furthermore, the length L_i of the folded arm modifies the coupling coefficient by varying the length of the coupled section [17]. The folded Y-shape isolator is also introducing the additional coupling path between the radiators resulting in the cancellation of mutual coupling between the radiators [18].

A. Effects of the Meander Line Conductor

The parametric study of the length L_r was conducted to first analyze the effects of varying the length on the resonant frequency. The results of the parametric analysis are shown in Figs. 2(a) and (b). The length of the meander line was varied from 6.4 mm to 7.2 mm. For smaller values of length, the resonance shifts to higher frequencies and for larger values of length the resonance shifts to lower frequencies. The length was optimized at 6.8 mm to achieve the optimum radiating band of 5.55 GHz with an $|S_{11}|$ of better than 20 dB and an isolation better than 15 dB. The dimensions of the folded Y-shape isolator were kept constant, as shown in Fig. 1(a), during the parametric analysis. Finally, it should be noted that the lower band was unaffected for various values of L_r.

B. Effect of Folded Y Isolator

Next, to achieve resonance at the lower frequency band, the dimensions of the folded Y-shape isolator were optimized. The length L_i of the folded section of the isolator and gap G_c can be adjusted to achieve the desired response by varying the edge coupling between the radiator edges and isolator. The gap G_c was kept constant and the length L_i of the folded arm was varied from 3.5 mm to 7.5 mm. The results of these variations are shown in Figs. 2(c) and (d). The folded Y-shape structure also acts as an isolator which provides an extra path for coupling fields to introduce current with opposite phase. The port isolation is strongly dependent on the total length of the folded Y-shape isolator which was kept at $\lambda_g/2$. Since the gap G_c between the two arms of the folded Y-shape isolator effects the electrical length of the isolator by producing mutual coupling between the arms; as a result the stub is slightly larger in length. Finally, it should be mentioned that the upper band was fixed for this parametric study, indicating the introduction of the lower band by the folded Y-shape isolator.

III. Experimental and Simulated Results

A. Scattering Parameters

The proposed design in Fig. 1 was simulated in HFSS along with the SMA connector model. The prototype was designed on a Rogers TMM4 substrate. The thickness of the substrate was 0.8 mm with a dielectric constant of 4.5 and a loss tangent of 0.002. The photograph of the fabricated prototype is shown in Fig. 3 and the measured and simulated results are plotted in Fig. 4. It should be noted that semi-rigid cables were connected to the bottom side of the prototype for measurements. It is shown that the isolation is better than 25 dB and 15 dB in the lower and higher bands, respectively. It can be observed from Fig. 4(a) that $|S_{22}|$ is less than 10 dB around 2.1 GHz but the structure is non-radiating in the region which was shown by measuring the gain at those frequency points. Although simulations were carried out with the SMA connector model, the compactness of the design makes it vulnerable to fabrication imperfections. Furthermore, the design involves vias which were soldered instead of platting so there was a change in inductance, hence this results in a slight resonant shift. Overall though, good agreement between simulation and measurements is shown, validating the HFSS model.

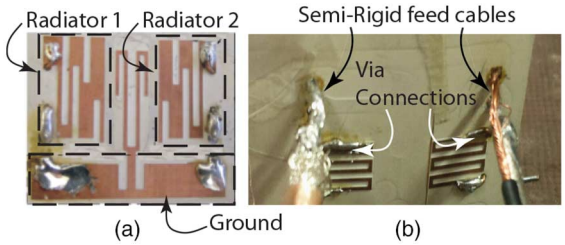

Fig. 3. Photograph of proposed dual band MIMO antenna: (a) top side and (b) bottom side.

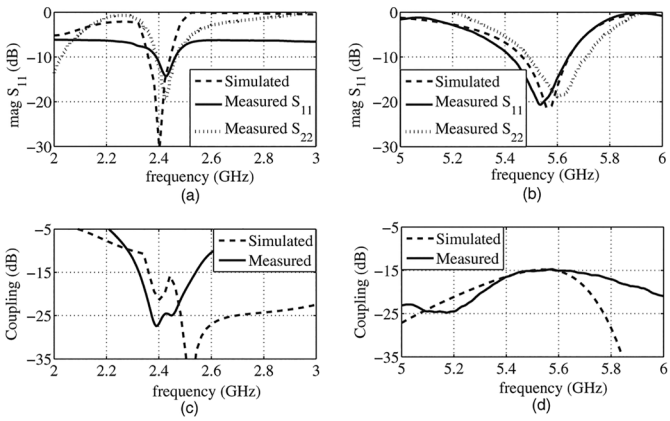

Fig. 4. Simulated and measured S-parameters of the dual band MIMO antenna array. (a) $|S_{11}|$ in the lower band, (b) $|S_{11}|$ in the higher band, (c) mutual coupling in the lower band and (d) mutual coupling in the higher band.

B. Radiation Pattern, Gain, and Efficiency

The radiation patterns of the proposed dual band MIMO antenna system were measured in the XZ, YZ and XY-planes in a fully calibrated anechoic chamber at 2.45 GHz and 5.55 GHz. The results were taken by driving port 1 and terminating port 2 with a 50Ω load and are shown in Fig. 5. Since the resonant frequency was shifted at the lower band, the measured results at 2.45 GHz were compared with the simulated results at 2.4 GHz. The simulated and measured radiation patterns are in agreement and a slight variation at certain angles are associated to imperfections in the realization of the prototype. The Omnidirectional behavior of the antenna is visible from the radiation patterns in Fig. 5. Next, the peak gain in the lower and higher bands of the antenna system are plotted in Figs. 6(a) and 6(b), respectively. Then, the total efficiency of the antenna was simulated and measured using the wheeler cap method [19]. The simulated total efficiency was computed to be 73% and 85% in the lower and higher bands, respectively; while the measured total efficiency was determined to be 64% and 71% in the lower and higher bands, respectively. The reduction in the total efficiency is due to the leakage of ground currents, the losses of the cap used for calculation and fabrication imperfections. As described earlier, the lower resonant band was shifted and the simulation results from 2.35 to 2.45 GHz are plotted in Fig. 6(a) along with the measured results from 2.4 to 2.5 GHz.

C. Diversity Analysis on Different Environments

The diversity performance of the proposed MIMO system has been carried out in different environments. The Envelope Correlation Coefficient (ECC) in the isotropic environment was mea-

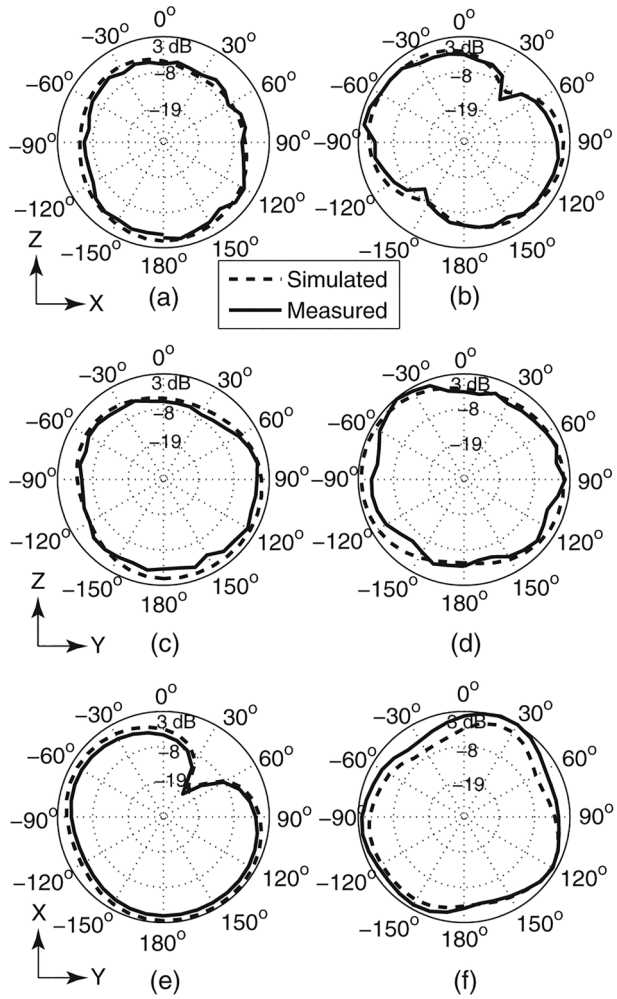

Fig. 5. Radiation pattern (a) XZ-plane at 2.45 GHz, (b) XZ-plane at 5.5 GHz, (c) YZ-plane at 2.45 GHz, (d) YZ-plane at 5.55 GHz, (e) XY-plane at 2.45 GHz and (f) XY-plane at 5.5 GHz.

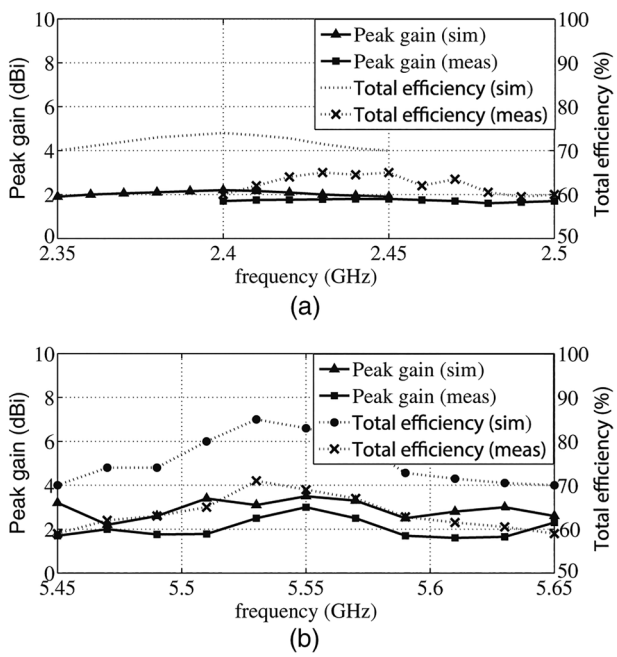

Fig. 6. Peak gain and total antenna efficiency: (a) lower band and (b) higher band.

TABLE I
PERFORMANCE COMPARISON WITH PREVIOUS PUBLISHED LITERATURE

Ref.	Size comp. (%)	BW (GHz)	Band Isolation (dB)	Peak Gain (dBi)/ Total effic. (%)	ECC (far-field pattern)
[5]	423	2.4 to 2.5	$<$ -15	0.98/ 49	N.A.
[6]	226	2.4 to 2.5	$<$ -20	1.57/ 75	N.A.
[13]	736	2.4 to 2.5/ 5.15 to 5.35	$<$ -20	2.5/41 (L.B)/ 0.3/42 (H.B)	$<$ 0.29
This work	100	2.4 to 2.5/ 5.4 to 5.8	$<$ -20 (L.B) $<$ -15 (H.B)	1.8/70 (L.B)/ 3/85 (H.B)	$<$ 0.1 (L.B)/ $<$ 0.07 (H.B)

sured using the S-parameters method proposed by Blanch *et al.* [20]. The measured ECC was less than 0.003 in both radiating bands. To further expand the analysis, the ECC was numerically calculated for indoor and outdoor environments using the far-field patterns [21]. For the lower band, the ECC was found to be less than 0.35 and 0.55 for indoor and outdoor environments, respectively. For the higher band, the values were less than 0.25 and 0.6 for indoor and outdoor environments, respectively. The multiplexing efficiency matrix, η_{MAX}, defines the difference in the power required for a MIMO antenna under-test (AUT) to obtain a given capacity relative to an ideal reference MIMO antenna of zero correlation and 100% total efficiency. Assuming a uniform 3D power spectrum and a high signal to noise ratio (SNR), η_{MAX} is given as [22]: $\eta_{MAX} = \sqrt{(1-|\rho_c|^2)\eta_1\eta_2}$ where ρ_c is a complex correlation coefficient which is the same as calculated from eqn. (1) in [12] for the isotropic case and it can also be approximated by ρ_e from the s-parameters $\rho_e = |\rho_c|^2$. Since $\rho_e < 1$ and the total efficiencies of both elements are the same, the calculated value of η_{MAX} remains above 95% indicating good MIMO performance of the proposed antenna design. Also, in Table I, a comparison of the overall performance of the proposed antenna system to previously published literature is presented. The area of the proposed antenna is much smaller and the overall performance is comparable or better than previous work with smaller dimensions.

IV. CONCLUSION

In this letter, a highly miniaturized dual band MIMO antenna is proposed for WLAN applications. The antenna operates from 2.4 GHz to 2.5 GHz and 5.45 GHz to 5.65 GHz. The resonances at these bands have been achieved by introducing the broadside and edge coupling in the structure. The measured $|S_{11}|$ and isolation is better than 10 dB and 15 dB in the lower and higher bands, respectively. Diversity analysis has also been carried out to check the performance of the proposed system in different environments. The antenna only measures $19 \times 23\ mm^2$, hence the planar geometry and small footprint of the antenna makes it suitable for compact devices as well as for USB dongle applications.

REFERENCES

[1] D. Gesbert, M. Shafi, D. Shiu, P. J. Smith, and A. Naguib, "From theory to practice: An overview of MIMO space-time coded wireless systems," *IEEE J. Sel. Areas Comm.*, vol. 2, no. 3, pp. 281–302, Apr. 2003.

[2] K.-J. Kim and K.-H. Ahn, "The high isolation dual-band inverted F antenna diversity system with the small N-section resonators on the ground plane," *Micr. Opt. Tech. Lett.*, vol. 49, no. 3, pp. 731–737, 2007.

[3] K.-J. Kim, W.-G. Lim, and J.-W. Yu, "High isolation internal dual-bandplanar inverted-F antenna diversity system with band-notched slots for MIMO terminals," in *Proc. 36th Eur. Micr. Conf.*, 2006, pp. 1414–1417.

[4] R. Makinen, V. Pynttari, J. Heikkinen, and M. Kivikoski, "Improvement of antenna isolation in hand-held devices using miniaturized electromagnetic band-gap structures," *Microw. Opt. Technol. Lett.*, vol. 49, no. 10, pp. 2508–2513, Oct. 2007.

[5] C. Y. Chiu, C. H. Cheng, R. D. Murchz, and C. R. Rowell, "Reduction of mutual coupling between closely-packed antenna elements," *IEEE Trans. Antennas Propag.*, vol. 55, no. 6, pp. 1732–1738, Jun. 2007.

[6] S. C. Chen, Y. S. Wang, and S. J. Chung, "A decoupling technique for increasing the port isolation between two strongly coupled antennas," *IEEE Trans. Antennas Propag.*, vol. 56, no. 12, pp. 3650–3658, 2008.

[7] A. Diallo, C. Luxey, P. Le Thuc, R. Staraj, and G. Kossiavas, "Enhanced two-antenna structures for UMTS diversity terminals," *IET Microw. Antennas Propag.*, vol. 2, no. 1, pp. 93–101, Feb. 2008.

[8] A. Chebihi, C. Luxey, A. Diallo, P. Le Thuc, and R. Staraj, "A novel isolation technique for closely spaced PIFAs for UMTS mobile phones," *IEEE Antennas Wireless Propag. Lett.*, vol. 7, pp. 665–668, 2008.

[9] Y. Li, Z. Zhang, W. Chen, Z. Feng, and M. F. Iskander, "A dual-polarization slot antenna using a compact CPW feeding structure," *IEEE Antennas Wireless Propag. Lett.*, vol. 9, pp. 191–194, 2010.

[10] Y. Li, Z. Zhang, J. Zheng, and Z. Feng, "Compact azimuthal omnidirectional dual-polarized antenna using highly isolated colocated slots," *IEEE Trans. Antennas and Propag.*, vol. 60, no. 9, pp. 4037–4045, Sep. 2012.

[11] S. Zhang, Z. Ying, J. Xiong, and H. Sailing, "Ultrawide band MIMO/Diversity antennas with a tree-like structure to enhance wideband isolation," *IEEE Antennas and Wireless Propag. lett.*, vol. 8, pp. 1279–1282, 2009.

[12] M. S. Khan, A. D. Capobiaco, A. I. Najam, I. Shoaib, E. Autizi, and M. F. Shafique, "Compact ultra-wideband diversity antenna with a floating parasitic digitated decoupling structure," in *IET Microwaves, Antenna and Propag.*, Mar. 2014.

[13] K. C. Lin, C. H. Wu, C. H. Lai, and T. G. Ma, "Novel dual-band decoupling network for two-element closely spaced array using synthesized microstrip lines," *IEEE Trans. Antennas Propag.*, vol. 60, no. 11, pp. 5118–5128, Nov. 2012.

[14] S. Zhang, B. K. Lau, A. Sunesson, and S. He, "Closely-packed UWB MIMO/diversity antenna with different patterns and polarizations for USB dongle applications," *IEEE Trans. Antennas Propag.*, vol. 60, no. 9, pp. 4372–4380, 2012.

[15] W. J. Liao, S. H. Chang, J. T. Yeh, and B. R. Hsiao, "Compact dual-band WLAN diversity antennas on USB dongle platform," *IEEE Trans. Antennas Propag.*, vol. 62, no. 1, pp. 109–118, 2014.

[16] M. Han and J. Choi, "Dual-band MIMO antenna using a symmetric slotted structure for 4G USB dongle application," in *IEEE Int. Symp. Antennas Propag.*, 2011, pp. 2223–2226.

[17] Z. Jin, J. H. Lim, and T. Y. Yun, "Small-size and high isolation MIMO antenna for WLAN," *J. ETRI*, vol. 34, no. 1, pp. 114–117, 2012.

[18] A. C. K. Mak, C. R. Rowell, and R. D. Murch, "Isolation Enhancement between two closely packed antennas," *IEEE Trans. Antennas Propag.*, vol. 56, no. 11, pp. 3411–3419, Nov. 2008.

[19] H. A. Wheeler, "The radiansphere around a small antenna," in *Proc. IRF*, Aug. 1959, pp. 1325–1331.

[20] S. Blanch, J. Romeu, and I. Corbella, "Exact representation of antenna system diversity performance from input parameter description," *Electron. Lett.*, vol. 39, no. 9, pp. 705–707, 2003.

[21] T. Taga, "Indoor measurement method for evaluating statistical distribution of incident waves under out-of-sight condition and experimental studies of characteristics of mobile station polarization diversity," *IEICE Trans.*, vol. J74-B-II, no. 11, pp. 608–615, 1991.

[22] R. Tian, B. K. Lau, and Z. Ying, "Multiplexing efficiency of MIMO antennas," *IEEE Antennas Wireless Propag. Lett.*, vol. 10, pp. 183–186, 2011.